to appear: J. Computer-Aided Surgery

Robotic Motion Compensation for Respiratory Movement during Radiosurgery

Achim Schweikard[1] Greg Glosser[2] Mohan Bodduluri[2]
Martin Murphy[3] John R. Adler[4]

[1] Informatik, TU München, D-80290 München

[2] Accuray Inc., Sunnyvale, CA. 94086, USA

[3] Neurosurgery, Stanford University Medical Center, Stanford, CA. 94305, USA.

[3,4] Radiation Oncology, Stanford University Medical Center, Stanford, CA. 94305, USA.

February 4, 2000

Abstract

Tumors in the chest and the abdomen move during respiration. The ability of conventional radiation therapy systems to compensate for respiratory motion by moving the radiation source is inherently limited. Since safety margins currently used in radiation therapy increase the radiation dose by a very large amount, an accurate tracking method for following the motion of the tumor is of utmost clinical relevance. We investigate methods to compensate for respiratory motion using robotic radiosurgery. Thus, the therapeutic beam is moved by a robotic arm, and follows the moving target tumor. To determine the precise position of the moving target we combine infrared tracking with synchronized X-ray imaging. Infrared emitters are used to record the motion of the patient's skin surface. A stereo X-ray imaging system provides information about the location of internal markers. During an initialization phase (prior to treatment), the correlation between the motions observed by the two sensors (X-ray imaging and infrared tracking) is computed. This model is also continuously updated during treatment to compensate for other, non-respiratory motion. Experiments and clinical trials suggest that robot-based methods can substantially reduce the safety margins currently needed in radiation therapy.

1 Introduction

Surgery and radiation have been main-stays for the treatment of cancer for several decades. Because it is non-invasive and done on an outpatient basis, irradiation has

unique appeal as a cancer therapy. However, for solid tumors, the efficacy of irradiation correlates directly with the ability to precisely target the cancer, and thereby avoid damaging surrounding healthy tissue. Improved spatial accuracy facilitates maximally aggressive and effective treatment. While this objective has been largely achieved for brain tumors, especially when highly accurate stereotactic localization is used, the problem of achieving similar accuracy within regions of the body affected by respiratory motion has eluded easy solution. Were it possible to compensate for breathing movements, significantly more efficacious treatments for thoracic and abdominal cancer would become readily feasible.

Without compensation for respiratory motion, it is necessary to enlarge the target volume with a safety margin. This is done to ensure that the tumor will be contained within the region of treatment. Intra-treatment displacements of a target have been reported to exceed 3 cm in the abdomen, and 1 cm for the prostate [8, 10]. For small targets, an appropriate safety margin produces a very large increase in treated volume. This is illustrated in the following example.

Example: Consider a spherical tumor of radius 1 cm. The ratio between the radius and volume of a sphere is cubic. Thus a margin of 1 cm will cause an 8-fold increase in treated volume, which primarily involves healthy tissue. Furthermore, observed motion ranges (in excess of 3 cm) suggest that a 1 cm margin may not be sufficient in all cases. An enlarged margin of 2 cm would result in a 27-fold increase of dose in our example.

Thus, an accurate method capable of compensating for respiratory motion would be of utmost clinical relevance.

To achieve progress in this direction, two main difficulties must be addressed.

- The exact spatial position of the tumor must be determined in real-time. New sensor techniques for measuring external motion are sufficiently fast and accurate to report motion of the patient's skin surface. However, the target motion may not follow the same direction as the external motion.

- The radiation source must be moved in space to follow a prescribed motion with high precision.

External tracking of the patient's skin surface motion will generally not be sufficient to determine the precise target location (Figure 1). Thus, while the skin surface may move in vertical direction, the diaphragm can internally move in horizontal direction at the same time. Respiratory motion patterns vary considerably between patients. Inhalation can result in a curve motion that differs from the exhalation curve (hysteresis). Some sectors of the curve (exhalation) may be traversed faster than others (inhalation).

Our work has two goals: (1) Design and implement suitable sensor techniques for determining the precise real-time target position in the presence of breathing motion. (2) Establish that active compensation for breathing motion is possible with robotic radiosurgery.

The next section discusses our basic approach in the context of related work. Section 3 first gives an overview of our sensor system. The navigation method is then described in sections 3.1 and 3.2. Results of clinical trials and an experimental evaluation of hypotheses involved in the presented method are discussed in section 4.

2 Related Work

Registration and tracking of anatomical structures has been investigated by many research groups over the last decade. Most notably, navigation methods in orthopedic surgery have achieved considerable accuracy and are in widespread clinical use. Navigation methods based on implanted artificial fiducial markers allow for robust and practical procedures. Newer techniques in orthopedics attempt to obviate the need for artificial fiducials [4, 5, 14]. While orthopedic navigation relies on bone structures or fiducial markers for localization and registration, it is difficult to extend accurate navigation methods to soft tissue. Soft tissue is deform-able, and soft tissue structures are more difficult to detect with X-ray imaging than bones. Due to respiration and pulsation, images sequences have high dynamics. Despite these difficulties, promising in-vitro results for applications of surgical soft tissue navigation have been described in the literature (see e.g. [2]). However the latter methods address surgical navigation, and cannot be extended directly to radiation therapy.

In radiation therapy, the therapeutic beam is generated by a medical linear accelerator, and moved by a gantry mechanism. Due to ionizing radiation, the surgical team cannot be present in treatment room during treatment. Thus the entire treatment is planned in advance, and monitored via cameras from outside the treatment room. The planning process determines appropriate beam directions from which to target the tumor and respective intensities. Conventional radiation therapy with medical linear accelerators (LINAC-systems) uses a gantry with two axes of rotation [13]. This mechanical construction was designed to deliver radiation from several different directions during a single treatment. Its ability to compensate for target motion during treatment is inherently very limited.

Respiratory gating is a technique for addressing the problem of breathing motion with conventional LINAC-based radiation therapy. Gating techniques do not directly compensate for breathing motion. I.e., the therapeutic beam is not moved *during* activation. Instead the beam is switched off whenever the target is outside a predefined window. One of the disadvantages of gating techniques is the increase in treatment time. A second problem is the inherent inaccuracy of such an approach. One must ensure that the beam activation cycles can have sufficient length for obtaining a stable therapeutic beam.

Kubo and Hill [6] compare various external sensors (breath temperature sensor, strain gauge and spirometer) with respect to their suitability for respiratory gating. By measuring breath temperature, it is possible to determine whether the patient is inhaling or exhaling. It is verified in [6] that frequent activation/deactivation

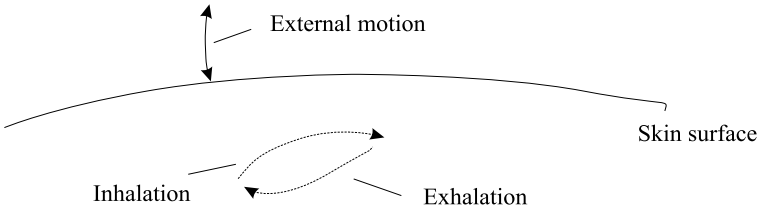

Figure 1: Tracking of external markers/motion curves corresponding to inhalation and exhalation. While external motion is in anterior/posterior direction, the internal motion of the target may be in left/right direction.

of the linear accelerator does not substantially affect the resulting dose distribution. However, the application of such a technique still requires a substantial safety margin.

Tada and Minakuchi et. al. [11] report using an external laser range sensor in connection with a LINAC-based system for respiratory gating. This device is used to switch the beam off whenever the sensor reports that the respiratory cycle is close to maximal inhalation or maximal exhalation.

Typical variations in the respiratory motion patterns of 1 to 2 cm for the same patient (in pediatrics), and in the duration of a single respiratory cycle of 2-5 seconds are reported in [10].

As noted above, the kinematics of conventional LINAC radiation systems with five motion axes is not suitable for tracking breathing motion. Conventional LINAC-systems have five motion axes. In principle, five axes are sufficient to target any point within a given workspace from any angle. However, four of the five axes of the LINAC-gantry are built into the patient couch. Thus, to compensate for respiratory motion it would be necessary to move the patient. Motions of the patient table (especially lateral table tilting) are likely to cause involuntary counter-motion of the patient. Such involuntary motions lead to muscle contraction, changes in breathing patterns, and may cause substantial inaccuracy.

LINAC-based systems are most widely used in radiation therapy. Given the kinematic limitations of such systems, most researchers have investigated methods for *motion detection* rather than active motion tracking.

A newer technique, based on a six degree-of-freedom robotic arm has been designed to improve radiosurgery for brain tumors (Cyberknife-system, Accuray Inc., Sunnyvale, CA. USA). This system employs a discretized treatment delivery scheme, and to date has been mainly used to treat tumors of the brain, head and neck region with stereotaxic radiosurgery [1, 9]. Thus, the beam is not moved during activation. Interestingly, a robotic gantry can move the beam in any direction during beam activation. All six motion axes move the radiation source, not the patient.

In this paper, we investigate a new method for soft tissue navigation in radiation therapy. Based on a modified Cyberknife robotic radiosurgery system, we combine stereo X-ray imaging with infrared tracking. X-ray imaging is used as an *internal* sensor, while infrared tracking provides information on the motion of the patient sur-

face. While X-ray imaging gives accurate information on the internal target location, it is not possible to obtain real-time motion information from X-ray imaging alone. In contrast, the motion of the patient surface can be tracked in real-time with commercial infrared position sensors. The central idea of our approach is to use a series of images from both sensors (infrared and X-ray) where image acquisition is *synchronized*. Thus, both X-ray image pairs and infrared data have *time-stamps*. From a series of sensor readings and corresponding time-stamps, we can determine a motion pattern. This pattern correlates external to internal motion, and is both patient- and site-specific. In a series of pre-clinical and clinical trials we verify that we can accurately infer the placement of an internal target tumor from the pre-computed (and continuously updated) motion pattern.

We then modify the robot-based treatment mode of the Cyberknife brain tumor protocol in such a way that respiratory motion can be compensated by active motion of the robot. Thus, it is not necessary to gate the beam.

3 Materials and Methods

3.1 Overview

Figure 2 shows the components of our system. A robot arm (modified Cyberknife system) moves a linear accelerator generating a 6 MV radiation beam. Infrared emitters are attached to a vest. An infrared tracking system records *external* motion of the patient's abdomen. An X-ray camera system (two X-ray cameras with nearly orthogonal visual axes) records the position of *internal* gold markers.

The following approach to respiratory tracking was investigated (fig. 3). Prior to treatment, small gold markers visible in X-ray images are attached to the target organ. Stereo X-ray imaging is used *during treatment* to determine the precise spatial location of the implanted gold markers via automated image analysis. Using stereo X-ray imaging, precise marker positions can be established once every 10 seconds. This time interval is too long to accurately following breathing motion.

In contrast, external markers (placed on the patient's skin) can be tracked automatically with optical methods at very high speed. Updated positions can be reported to the control computer more than 60 times per second. As noted above, external markers alone cannot adequately reflect internal displacements caused by breathing motion. Large external motion may occur together with very small internal motion, and vice versa. In addition the direction of the visible external motion may deviate substantially from the direction of the target motion.

Because neither internal nor external markers alone are sufficient for accurate tracking of lesions near the diaphragm, X-ray imaging is synchronized with optical tracking of external markers. The external markers are small active infrared emitters (IGT Flashpoint 5000, Boulder, CO.) attached to a vest. Notice that the individual markers are allowed to change their relative placement. The first step during

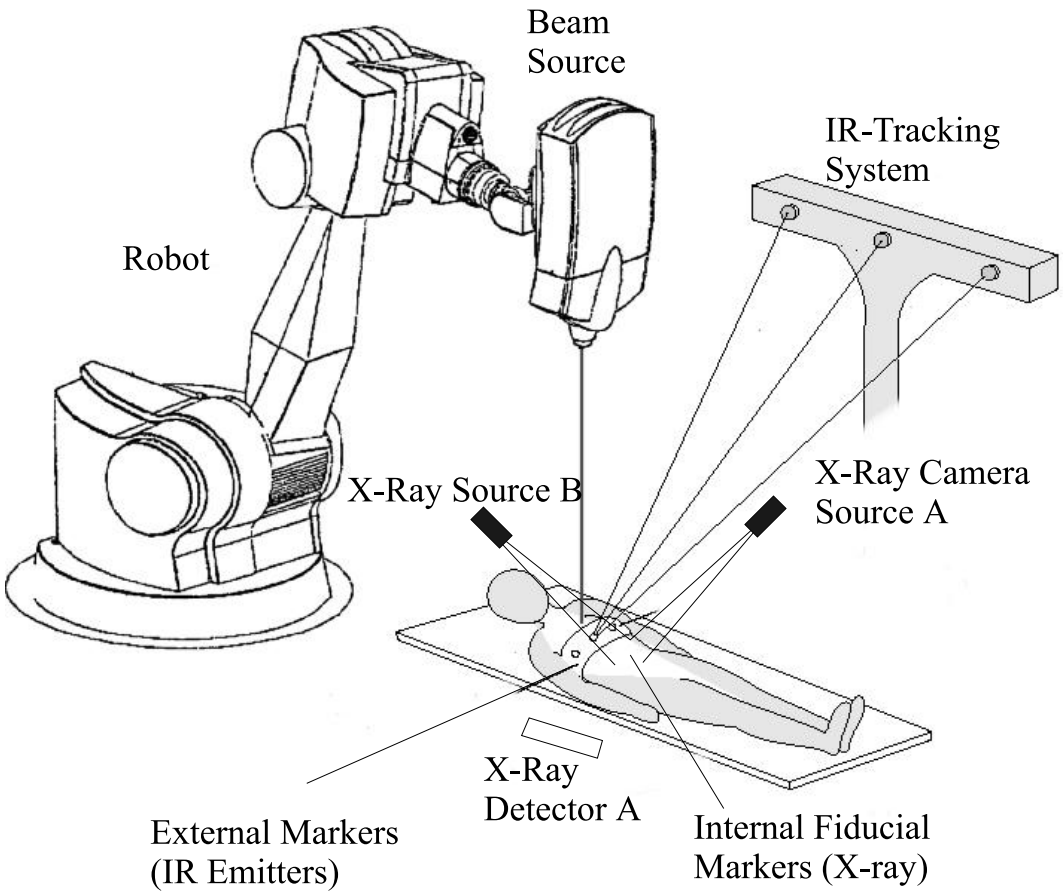

Figure 2: System overview. Infrared tracking is used to record *external* motion of the patient's abdominal and chest surface. Stereo X-ray imaging is used to record the 3-dimensional position of *internal* markers (gold fiducials) at fixed time intervals during treatment. A robotic arm moves the beam source to actively compensate for respiratory motion.

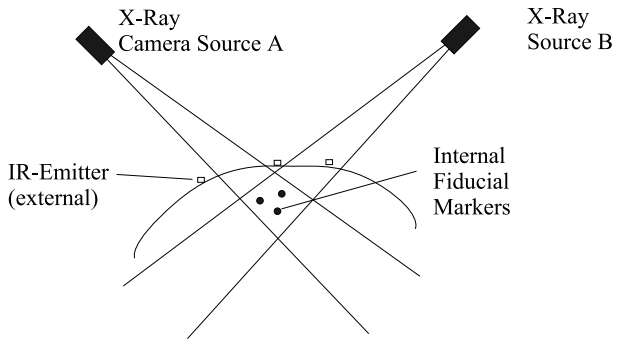

Figure 3: Sensor system. Correlation between motion of internal and external markers is computed prior to treatment and updated during treatment.

treatment is to compute the exact relationship between internal and external motion, using a series of time-stamped snapshots showing external and internal markers simultaneously.

Although the infrared tracking is combined with X-ray imaging, it is not necessary to detect to position of the infrared emitters in an X-ray image. Time-stamps permit the *simultaneous* positions of both marker types to be established, and can therefore be used to determine respiratory motion patterns. These motion patterns are patient-specific, and can be updated during treatment.

3.2 Computation of a Deformation Model

During the initialization stage of the procedure, a deformation model is computed, which describes the correlation between internal and external motion. To obtain the deformation model, we proceed as follows. A series of (stereo) X-ray image pairs of the target region are taken while the patient is breathing. When activating the X-ray sources, we record the time of activation. We also record the current position of the external sensors at the time of X-ray image acquisition.

Assume five X-ray image pairs have been taken in this way. These images have a sequence order, namely the sequence in which they were taken. In each image, we compute the position of the gold markers. Note that we obtain their exact *spatial* position, since the X-ray imaging reports stereo images. Consider the first of the gold markers. By linear interpolation, the positions of this marker determine a curve in space. We compute such an interpolation curve for each of the gold markers.

There are six *external* markers, and we compute the center of mass for these markers. During a motion, the series of center points thus obtained gives rise to a single curve describing the motion of the external markers. As the treatment proceeds the curves for internal and external markers are used in the following way. A new pair of X-ray images is acquired every 10 seconds. Let t be a time point, at which no X-ray image is taken. We must then determine a *predicted* target placement based on the given deformation model. At the given time point t, we read the external sensor positions. After computing the center of mass for the external markers, we can locate the closest point on the curve for the external motion in our deformation model. By linear interpolation this point determines corresponding points on the curves for the internal markers.

To simplify the description, we consider two such curves (one external, one internal) and assume both curves are line segments. Thus, assume the external curve is a segment with the two endpoints p and p' and the internal curve has endpoints q, q'. We now encounter the external marker at time point t in position x. The value λ, for which the point $p + \lambda(p' - p)$ has minimal distance from x determines a point x' on the line segment q, q'. Thus, linear interpolation yields $x' = q + \lambda(q' - q)$ as predicted internal location.

This simple linear interpolation extends directly to the case, where one or both curves are not line segments. In this case, points are connected by line segments,

and we determine the lengths of the line segments in each curve. The parameter interval $[0, 1]$ for each curve is then partitioned according to these lengths, and the interpolation proceeds as above. This interpolation is sufficiently fast to update the given deformation model as the treatment proceeds. Specifically, as new X-ray images and matching sensor readings become available, the curves for the internal markers are updated. The updating scheme will be described in more detail in the next two sections.

3.3 Detecting Patient Motion

A difficulty arising in this context is to distinguish between patient movement and breathing motion. Clearly, the two types of motion must be processed in different ways. Patient movement can occur, e.g., as a result of muscle relaxation, sneezing, or voluntary movement. A patient shift must cause a shift of the deformation model, i.e., each curve must be shifted. In contrast, normal breathing should not shift these curves.

3.3.1 Comparing predicted and actual marker placement

At first glance, distinguishing the two types of motion may seem difficult. However the internal markers represent a 'ground truth'. Thus, our deformation model gives a *predicted* position for the internal markers, based on the position of the external markers. The location of internal markers can be predicted not only for time points *in between* X-ray imaging, but also for the times *at which images are taken*. Any deviation (exceeding a fixed threshold value δ) between predicted and actual placement is thus regarded as displacement caused by patient motion. Thus, the above linear interpolation scheme yields a predicted placement for each internal marker. This predicted placement is a point in space. We compute the distance from the actual placement of this point. If this distance is larger than δ, the beam is switched off. A new deformation model is computed after respiration has stabilized.

Small values for δ give better accuracy, but enforce frequent re-computations of the deformation model. Given differences in patterns of breathing between patients, it is reasonable to determine an appropriate value for δ during initialization, when the patient is asked to breathe regularly. The deviations observed during this interval of regular breathing (here for the external sensors alone) are used to determine δ.

3.3.2 Practical Improvements

A practical improvement of this technique for detecting patient motion allows for updating the deformation model without interrupting the treatment. Assume the deformation model consists of five X-ray image pairs together with matching infrared position data. Since we take a new pair of X-ray images at fixed time intervals during treatment (i.e., every 10 seconds), the deformation model can be updated continuously

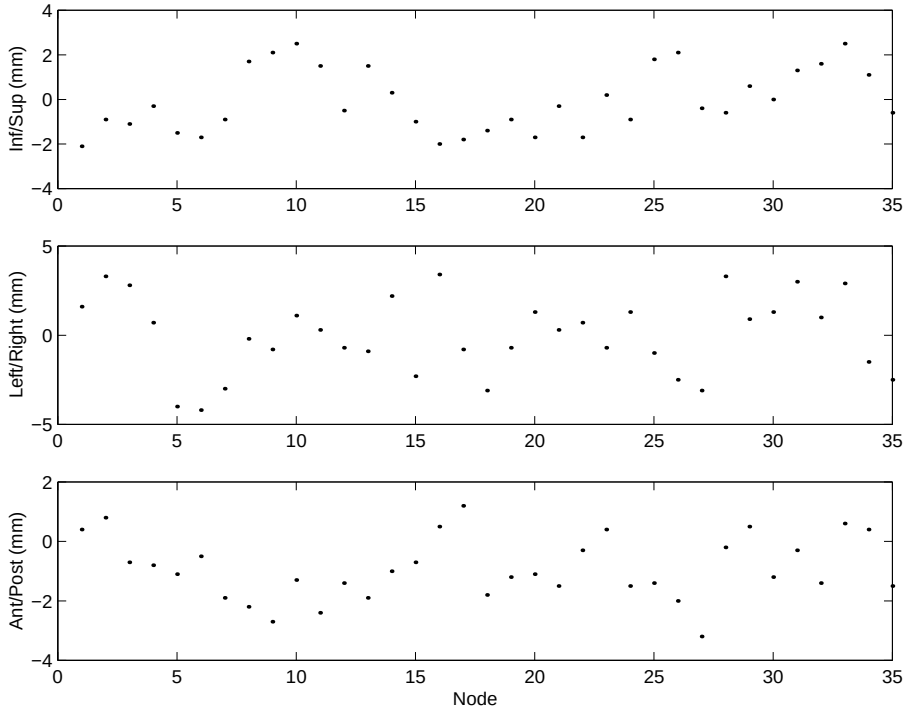

Figure 4: Fiducial tracking (pancreatic cancer). The patient was asked to hold her breath at a predefined reference location. Measured deviations from the reference location in three translational directions (35 beam activation phases).

in the following way. A table of position data with five entries is maintained. Each entry has a time-stamp. In this table, we remove the earliest entry whenever a new set of position data (image pair with matching infrared positions) becomes available. The computation of the deformation model via linear interpolation can be carried out in real-time after each update of the table data. This method can compensate both for systematic drift of the patient position and for small changes in the pattern of respiration during treatment.

4 Results

4.1 Clinical Trials

A first clinical trial was performed with fiducial tracking only. A patient with pancreatic cancer was treated while using X-ray imaging to monitor the position of the pancreas during treatment. Four gold markers with 2.5 mm diameter were sutured into the tissue surrounding the tumor during exploratory pre-treatment laparotomy. The goal of this trial was to measure the motion range for the pancreas, and to test the reliability of fiducial detection under treatment conditions.

During treatment, intra-operative stereo X-ray images were taken at fixed time intervals. In this case, the spatial coordinates of the fiducials can be computed. The patient attempted to hold her breath at approximately the same position immediately before imaging. A position close to full exhalation was defined as a reference position. The patient was asked to remain at the reference position as closely as possible during the entire beam activation period of 15 seconds. The displacement computed from the X-ray images was used to reposition the robotic arm in order to reach and maintain alignment with the target during beam activation. Figure 4 shows the displacements encountered for 35 beam activation phases. Notice that X-ray images were only taken immediately before, but not during beam activation phases. The abscissa values index the image pairs, i.e., each abscissa value corresponds to one image pair. For each such image pair, the figure gives the displacement signals sent to the robot for repositioning the beam along three translational axes. The measurements reveal that considerable inaccuracy remains even when the patient attempts to assiduously return to the same position in the respiratory cycle.

The procedure used in this trial requires that the patient holds her breath for an extended period of time. Since this can involve muscular tension and/or muscle relaxation, the exact internal positions are more difficult to infer from a deformation model. Larger displacements can occur as a result of muscle relaxation. Thus, muscular motion may occur instead of respiratory motion. The experiment demonstrates that the automatic detection and position computation of fiducial markers is practical. However, the necessary resting periods between beam activation/breath-holding cause a substantial increase in treatment time. Total treatment time in this first case was over 4 hours. This suggests that tracking the tumor by moving the beam could substantially simplify the procedure.

A second experiment analyzes the correlation between internal and external motion. For a second patient with pancreatic cancer X-ray image pairs were taken while the patient was breathing normally. For this patient small surgical skin staples (placed during preceding surgery to close an opening) were visible in the X-ray images (fig. 5). Notice that the staples are on the skin surface. Therefore, we can detect both internal *and* external motion in the X-ray image alone. Thus, instead of synchronizing the two sensors (infrared and X-ray) with high accuracy, we can simply use X-ray image pairs to analyze the correlation between internal and external motion. In our experiment, we can thus determine this correlation, while ensuring that there are no errors due to inaccurate synchronization.

To verify that the motion of the patient's skin surface is indeed correlated to the internal motion, the images were analyzed in the following way. For each image, the exact location of one of the staples and of the four implanted gold fiducial markers was computed. We then used this data to predict the positions of the internal fiducials from the observed positions of the staple. The results are summarized in fig. 6 and 7. To analyze the data, we regard the absolute displacement of the fiducial's center of mass as $x-$coordinate of one data point. The absolute displacement of the staple in the same image then gives the y-coordinate of the same data point. A total of 50

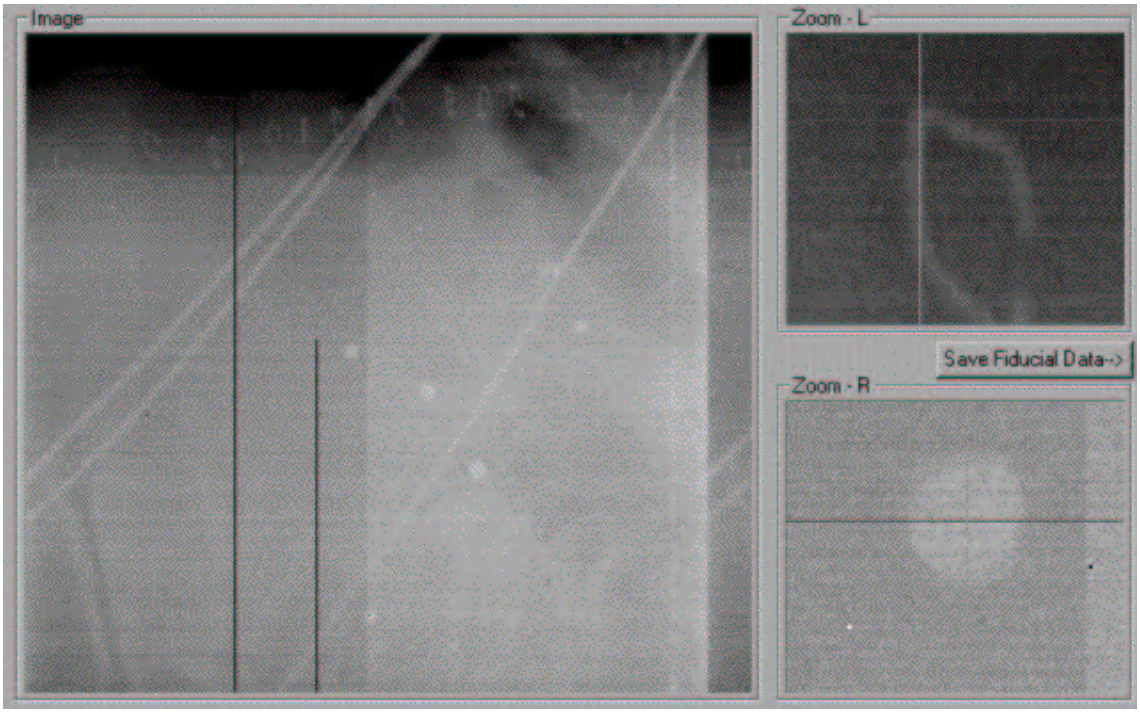

Figure 5: X-ray image with internal fiducial markers. Left image: small staples are used to determine external motion. Right images: staple and fiducial marker.

x-ray image pairs was analyzed in this way. A regression line for the two-dimensional point data was then computed. The RMS error for pointwise deviation from this regression line was 0.61mm.

4.2 Sensor System

To verify the stability of the infrared tracking system in the presence of radiation, infrared emitters were directly exposed to the therapeutic beam (6 MV radiation beam) for an extended period of time. The infrared system showed a noise range of less than 0.01 mm (with emitters and camera fixed). No increase in noise was observed during the radiation exposure. This suggests that infrared tracking is an adequate position sensor for radiation therapy.

Our tracking method relies on the hypothesis that the simultaneous motion of the external and internal markers (represented by gold markers and infrared emitters) follows a consistent and reproducible pattern. To test this hypothesis on large data sets, without exposing subjects to elevated radiation doses from x-ray imaging, the following set-up was used. Three external markers were placed on a subject's chest surface. A second set of external markers was placed on the subject's abdomen. With the subject breathing regularly, the positions of both marker sets were recorded. After an initialization phase, the abdominal movement itself was used to *predict*

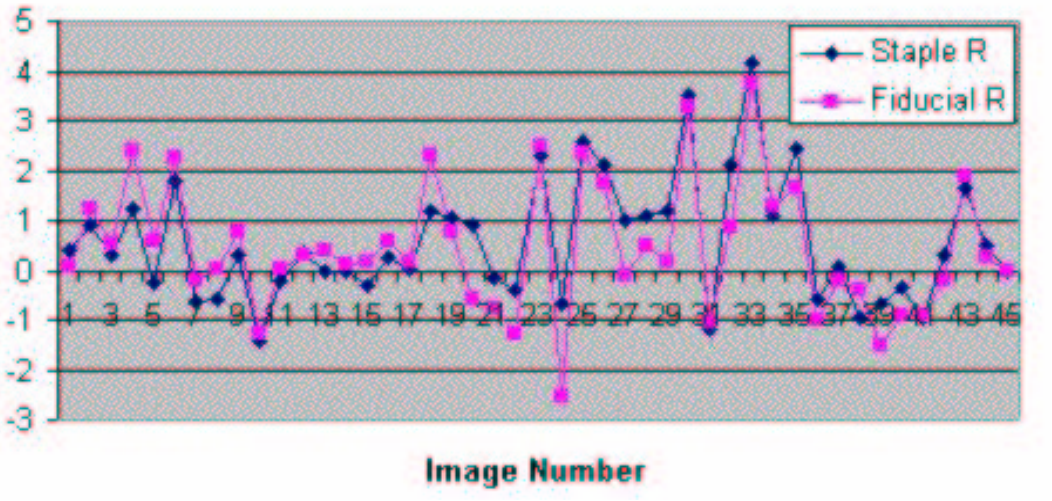

Figure 6: Correlation between internal an external motion (Pancreatic cancer patient, Stanford Medical Center). Displacements (in mm) of the staple are shown together with displacements of the center of mass of the four fiducial markers.

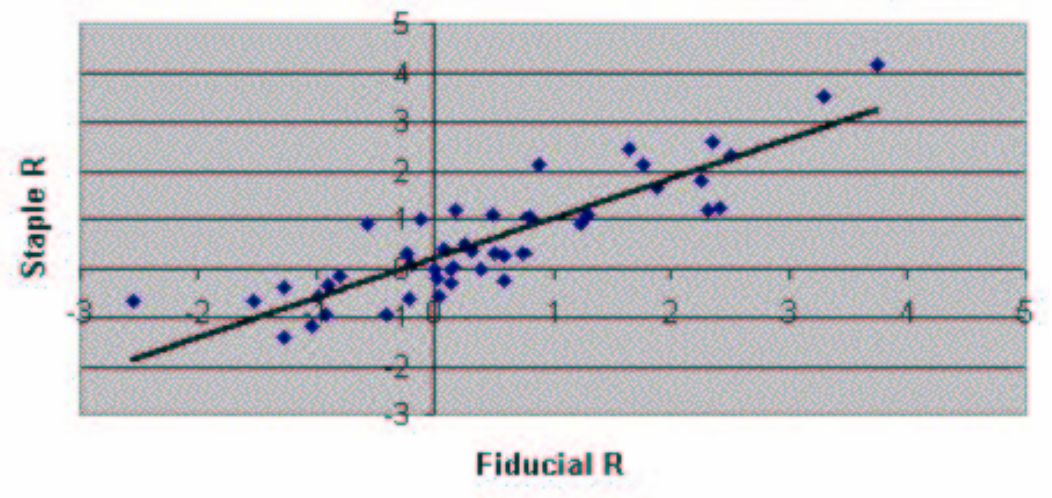

Figure 7: Correlation between internal and external motion. Absolute displacement of a staple on the patient's skin, correlated with absolute displacement of one internal fiducial marker (in mm).

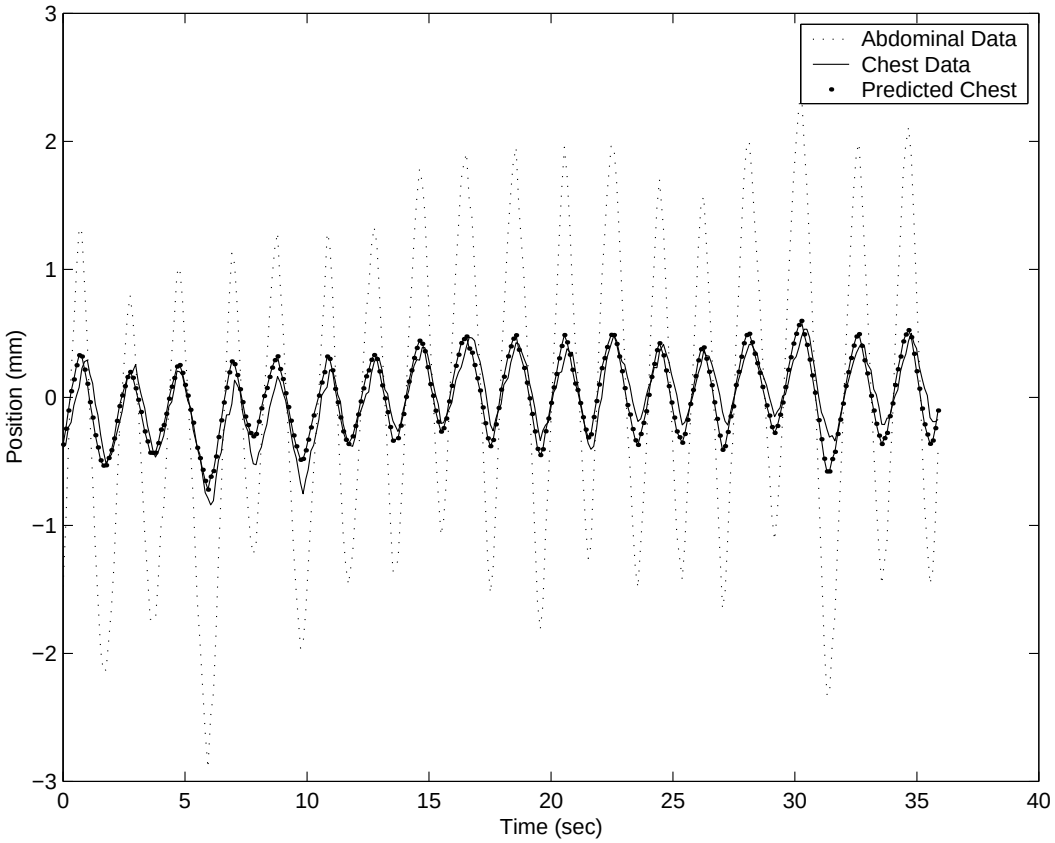

Figure 8: Motion curves for abdominal and chest motion. Solid line: actual motion curve for chest motion. Solid line with dots: predicted curve for chest motion. Prediction computed from 5 data points taken during initialization.

the motion of the chest surface, thereby providing real-time information of both the actual *and* the predicted motion of the chest markers. The two resulting position curves (predicted and actual) were then evaluated for their dependency upon the number of 'snapshots' used in the computation of the deformation model. Thus, we first compute a deformation model from a *training set* of only five data points. At each time point in the training set, the simultaneous positions of one chest marker and one abdominal marker are recorded. With this training set (consisting of five points) we predict the subsequent motion of the chest markers. The corresponding position curves are shown in figure 8.

Figure 9 shows the measured error as a function of the number of time points. The accuracy is first determined for 2 sample points, and continues in increments of five points. These measurements confirm our hypothesis that only a few time points are sufficient for predicting the chest motion from observed abdominal motion with high accuracy (< 0.2 mm).

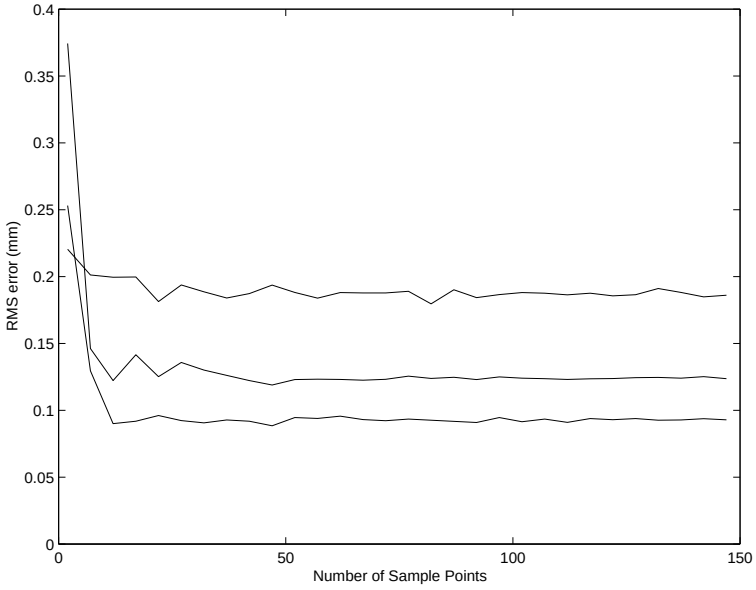

Figure 9: Root mean squared error in predicted chest motion. Abscissa values: number of time points in training data set. The three curves correspond to three different infrared emitters. In each case, the same emitter on the abdomen was used to infer the position of one of the three emitters on the chest.

4.3 Accuracy of Motion Tracking

To measure the required speed for compensating respiratory motion, the velocity of the external motion visible on the patient's chest/abdomen was measured. A subject wearing the vest with infrared emitters (section 3.1) was asked to breathe regularly while laying on a patient table. The motion of the infrared emitters on the vest was recorded and the resulting velocity was computed. Figure 10 shows the results of this measurement. The position curves show the absolute position of the markers as a function of time (given in seconds on the abscissa). To calculate absolute positions, the (3D) displacement from the initial position (time s = 0) was used. Figure 11 displays the simultaneous position of the six external markers over the same respiratory cycles as in figure 10. Experiments carried out for 10 subjects suggest, that a maximum velocity of 12 mm/sec is sufficient for tracking external motion.

The weight of the linear accelerator causes large inertial forces. To determine the motion lag of the robotic gantry (GM Fanuc 430 robot), an infrared probe was attached to the linear accelerator (moved by the robot). A thin laser beam, pointing along the therapeutic beam's central axis indicates the current pointing direction of the linear accelerator (with beam off). A hand-held needle pointer, equipped with infrared emitters was used to prescribe points and motions in space.

While waving the hand-held needle pointer the robot tracked its motion. The

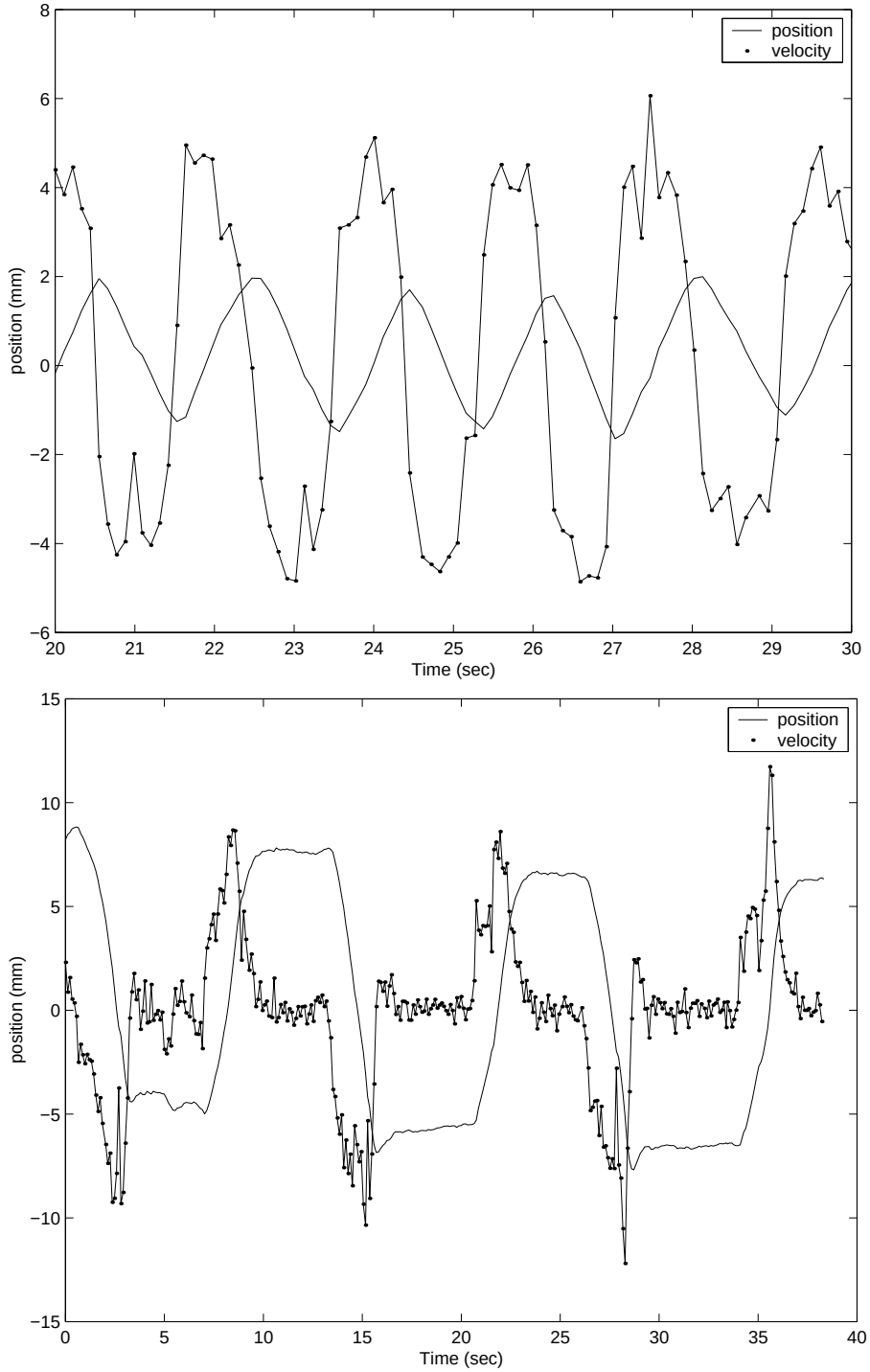

Figure 10: External marker displacement and velocity: (a) normal breathing, (b) deep breathing.

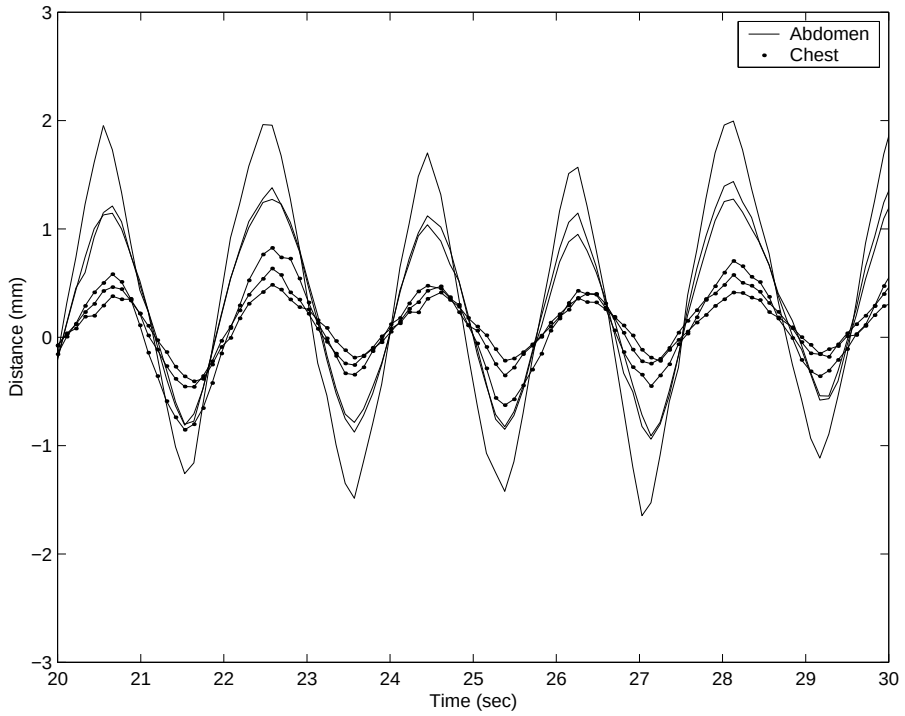

Figure 11: External respiratory motion. Three markers attached to the chest, three markers attached to the abdomen. The data set is the same as in figure 10-a.

tracking accuracy was verified by the laser beam, moved by the robot. If the tracking is sufficiently accurate and fast, the laser beam will cross and illuminate the needle tip during the entire motion. The tracking accuracy was not only verified visually, i.e., by checking whether the laser illuminates the needle tip, but also with the infrared tracking system. Recall that infrared emitters are attached to both the moving needle pointer and to the laser source held by the robot. Thus we can write the position data of both the laser and the needle to a file. Post-processing this file allowed deviation between actual and commanded position/velocity to be determined.

To prescribe a linear motion with predetermined velocity, we attached the needle pointer to a numerically controlled motion table. Figure 12 shows the set-up used in this experiment. The motion table was then moved at different velocities, the range of which corresponded to that observed for breathing (figure 10). Figure 13 shows the motion curves for both the robot and needle pointer. The motions are very regular, since the needle pointer was attached to the motion table. A systematic lag was found to cause a displacement consistent with the corresponding velocity. We currently do not compensate for this lag by predicting motions, although the regularity of breathing patterns may allow for such a prediction to a limited extent in the future. Table 1 shows the motion lag of the robot following the needle tip (in mm, calculated as root of mean of squared errors) for linear motions of the needle pointer.

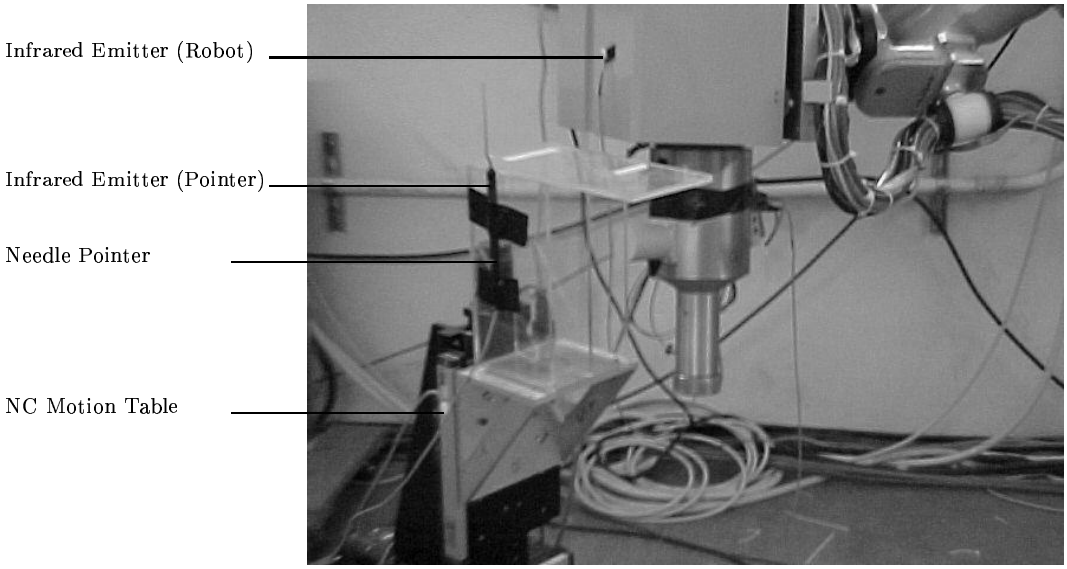

Figure 12: Tracking a linear motion with velocity prescribed by a motion table.

v	RMS Error	Time Lag	Phase Shift
3mm/s	0.9 mm	0.33 s	8.9 deg.
6mm/s	1.8 mm	0.30 s	16.5 deg.
10mm/s	2.8 mm	0.30 s	25.2 deg.

Table 1: Accuracy of motion tracking (mm). Robot arm with linear accelerator is tracking the motion of a needle pointer attached to a motion table.

We then placed the needle pointer on a subject's chest. In this case, compensating robot motion must follow a curve in 3D. The observed motion curves for chest motion and robot motion are shown in figure 14. This figure shows lags for various sections of the curve with different velocities. The results show that typical respiratory velocity of 2-4 mm/sec result in a (systematic) lag between 1 and 2 mm.

5 Discussion and Conclusions

The described technique combines information from two sensors: X-ray imaging and infrared tracking. Both sensors have very characteristic advantages in our application. Stereo X-ray imaging can determine the exact location of fiducial markers via automatic image analysis. Our tracking method (X-ray imaging with time-stamps, combined with infrared sensing) does not require the location of the infrared emitters be computed in the X-ray images. The infrared emitters do not even have to be visible in the X-ray images. This avoids occlusions and simplifies image processing considerably. The observed motions of external infrared markers (4 mm to 20 mm) is large when compared to the noise range of infrared position computation (below 0.01

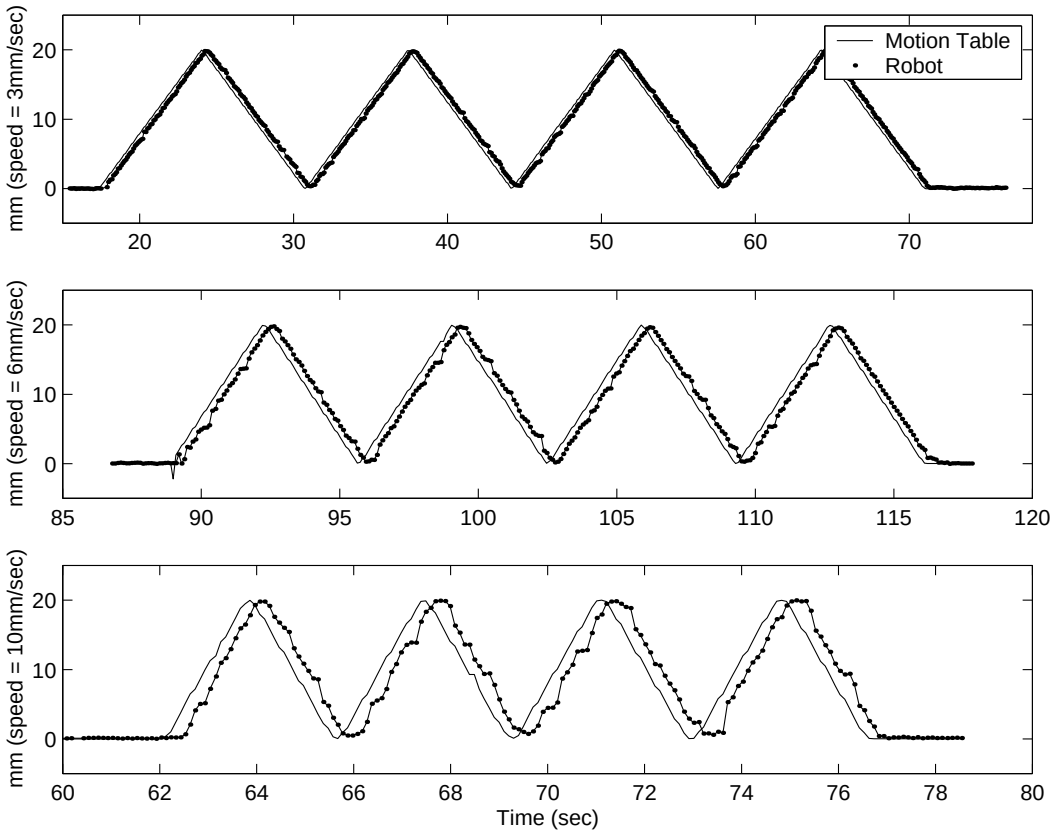

Figure 13: Tracking a linear motion with velocity prescribed by a motion table. Velocity 3, 6 and 10 mm/sec. Motion range 20 mm.

mm). Thus, the ratio between noise and signal is adequate for following the respiratory cycle. High accuracy and speed as well as stability under radiation exposure are further advantages of infrared tracking in our application. Intervals of in the range of 10 seconds were used for X-ray image acquisition. While it seems possible to shorten this interval in the future, the 10-second imaging intervals are currently necessary for several reasons. Firstly, overheating of the X-ray sources must be avoided. Secondly, even much shorter imaging intervals (such as one-second intervals) would not be sufficient for tracking respiratory motion accurately with X-ray imaging alone. Finally, while the radiation dose stemming from the cameras is very small when compared to the therapeutic beam, such radiation should not be applied without necessity.

Our method currently requires fiducial markers be implanted prior to treatment. While this procedure is more invasive than direct (non-stereotaxic) radiation therapy, the gain in localization accuracy should justify this added invasiveness. It is possible that advanced image processing methods can ultimately obviate the need for implanted fiducial markers.

Since patient motion can directly influence robot motion, it is necessary to prevent collisions in the workspace. Currently, the compensating motions are limited to 5 cm.

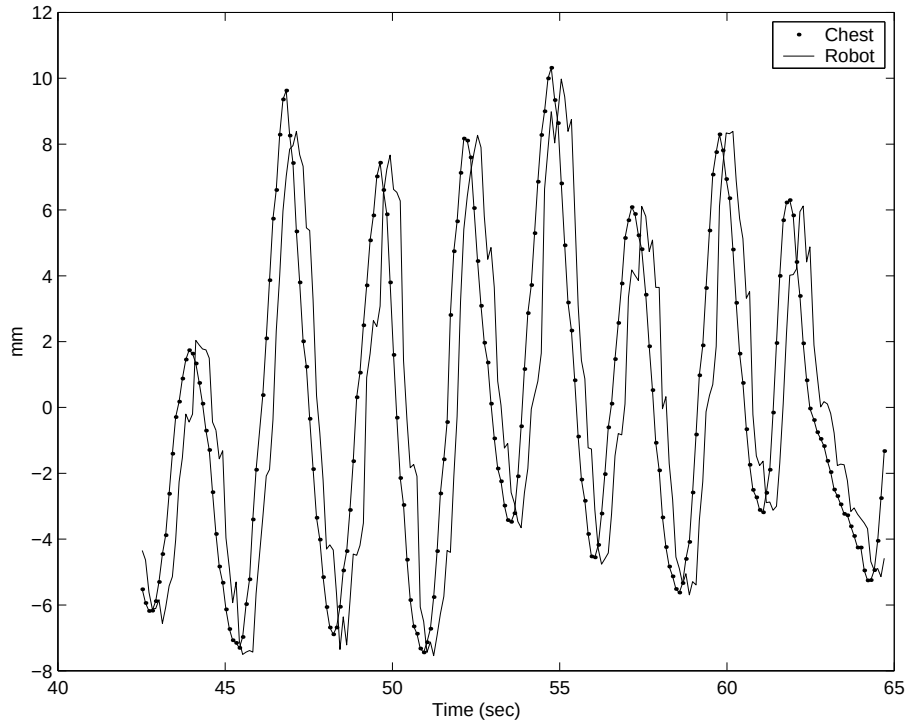

Figure 14: Tracking respiratory motion with the robot arm. Infrared emitter attached to a test person during breathing.

The workspace is analyzed by an offline kinematic simulation program, thus ensuring that no collisions can occur during compensating motions.

The experiments confirm our hypothesis that respiratory motion of internal organs can be correlated to visible external motion, provided that the correlation model can be updated automatically in real-time by intra-operative images. This suggests that any dose margin placed around a tumor to compensate for respiratory motion can be reduced by a very substantial amount. Since dose is directly proportional to volume, this could allow for higher doses in the tumor, and much lower dose in surrounding healthy tissue. For a variety of cancers with grim prognosis, this robotic technique could thus lead to far-reaching improvements in clinical outcome.

References

[1] Adler, J. R., Schweikard, A., Tombropoulos, R., Latombe, J.-C., Image-Guided Robotic Radiosurgery. In: *Radiosurgery*, Kondziolka, (ed.) New York: Karger Medical and Scientific, 1999.

[2] Bzostek, a., Inoescu, G., Carrat, L., Barbe, C., Chavanon, O., Troccaz, J. Isolating Moving Anatomy in Ultrasound without Anatomical Knowledge: Application

to Computer-Assisted Pericardical Punctures. Medical Image-Computation and Computer-Assisted Intervention - MICCAI 98, Lecture Notes in Computer Science, vol. 1496, 1041–1048, 1998.

[3] Carol, M. P., Targovnik, H.,: 3D planning and delivery system for optimized conformal therapy. *Int. J. Radiat. Oncol. Biol. Phys.*, 24, 1992.

[4] R. Hofstetter, M. Slomoczykowski, M. Bourquin, L. P. Nolte, Flouroscopy-based surgical navigation - concept and clinical applications. Computer-Assisted Radiology and Surgery (CAR), Lemke, H.U., Vannier, M., Inamura, K., (ed.), Elsevier Science, p. 956 - 960, 1997.

[5] R. Hofstetter, M. Slomoczykowski, M. Sati, L. P. Nolte, Flouroscopy as an imaging means for Computer-Assisted Surgical Navigation. *Computer-Aided Surgery*, 4, 65-76, 1999.

[6] Kubo, H. D., and Hill, B. C., Respiration gated radiotherapy treatment: a technical study. *Phys. Med. Biol.*, 41, 93–91, 1996.

[7] Lujan, A. E., Larsen, E. W., Balter, J. M., Haken, R. K. T., A Method for incorporating Organ Motion due to Breathing into 3D Dose Calculations. *Medical Physics*, 26 (5), 715–720, 1999.

[8] Morrill, S. M., Langer, M., Lane, R. G., Real-Time Couch compensation for intra-treatment Organ Motion: Theoretical Advantages. *Medical Physics*, 23, 1083, 1996.

[9] Schweikard, A., Bodduluri, M., Adler, J. R., Planning for Camera-Guided Robotic Radiosurgery. *IEEE Trans. on Robotics and Automation*, 14, 6, 951–962, 1998.

[10] Sontag, M. R., Lai, Z. W., et. al., Characterization of Respiratory Motion for Pedriatic Conformal 3D Therapy. *Medical Physics*, 23, 1082, 1996.

[11] Tada, T., Minakuchi, K., et. al., Lung Cancer: Intermittent Irradiation Synchronized with Respiratory Motion - Results of a Pilot Study. *Radiology*, 207 (3), 779 - 783, 1998.

[12] Winston, K. R. and Lutz, W., Linear accelerator as a neurosurgical tool for stereotactic radiosurgery. *Neurosurgery*, 22(3):454–464, 1988.

[13] Webb, S.,: The Physics of Three-dimensional Radiation Therapy, Institute of Physics Publishing, Bristol and Philadelphia: 1993.

[14] Z. Yaniv, L. Joskowicz, A. Simkin, M. Garza-Jinich, C. Milgrom, Flouroscopic image processing for computer-aided orthopedic surgery. First Int. Conf. on Medical Computing and Computer-Assisted Intervention, Boston, p. 325 - 324, 1998.